Geothermics 114 (2023) 102785

Contents lists available at ScienceDirect

Geothermics

journal homepage: www.elsevier.com/locate/geothermics

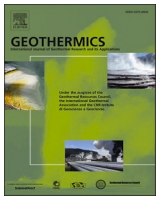

Influence of site characteristics on the performance of shallow borehole heat exchanger arrays: A sensitivity analysis

Quan Liu [a,*], Finn Weiland [b], Peter Pärisch [b], Niklas Kracht [b], Mu Huang [b], Thomas Ptak [a]

[a] Geoscience Center, University of Göttingen, Göttingen, Germany
[b] Institute for Solar Energy Research in Hamelin (ISFH), Emmerthal, Germany

ARTICLE INFO

Keywords:
Site characteristics
Borehole heat exchanger arrays
Sensitivity analysis
Annual heat production
Groundwater flow
Subsurface heterogeneity

ABSTRACT

Using borehole heat exchangers (BHE) to extract shallow geothermal energy has grown rapidly in recent years. How to maintain a long-term balanced, sustainable operation of the BHE arrays becomes a key issue. Site characteristics, including hydrogeological and geothermal conditions as well as spatial distribution of subsurface physical parameters, are generally idealized or partly neglected in practice. To investigate the consequences of such simplifications, a 3D model, based on data from a planned real site, is established to consider groundwater flow, subsurface heterogeneity, and various hydrogeothermal boundary conditions. After verifying the model, a sensitivity analysis is conducted. Nine factors regarding site characteristics are selected, including Darcy flux in the aquifer, thermal conductivity and volumetric heat capacity of the ground, groundwater depth, thermal and hydraulic heterogeneity, geothermal gradient, heat transfer coefficient on the ground surface and seasonal rainfall. Sensitivity results indicate that the annual total heat production is most sensitive to geothermal gradient, followed by Darcy flux, both of which have positive effects. Groundwater depth and heat transfer coefficient have negative effects on annual heat production. Compared to thermal heterogeneity and rainfall, the influence of hydraulic heterogeneity is higher. Uncertainty of annual heat production due to various Peclet numbers is quantified through regression analysis.

1. Introduction

Shallow geothermal energy has attracted extensive attention as an alternative and renewable energy source for comfort heating and cooling of buildings. Especially in the past ten years, to alleviate the contradiction between growing energy demand and environmental issues, borehole heat exchangers (BHE) are widely used and have become one of the most common heat sources for geothermal heat pumps (GHP). However, during long-term GHP operation, negative performance, i.e. production decline, can be observed in practice (Bassetti et al., 2006; Florea et al., 2017) and stimulates intensive discussion (Hein et al., 2016; Schincariol and Raymond, 2021). Thermal non-equilibrium within the BHE array during long-term operation is thought to be the major reason (Rybach and Eugster, 2002; Signorelli et al., 2004).

In a well-designed GHP system, site characteristics, including hydrogeological and geothermal conditions and subsurface physical parameter fields, can be the major source of uncertainty impacting on the thermal equilibrium of the BHE array (Stauffer et al., 2013). The reason is that site properties are generally underexplored due cost-minimizing of GHP systems, and therefore being represented by idealized assumptions during the design process. For instance, groundwater flow is often neglected and the hydrogeological and geothermal parameters are usually assumed to be homogeneously distributed (Pärisch et al., 2015; Rivera et al., 2016). However, many studies showed that groundwater flow can be a significant factor of BHE performance (Al-Khoury et al., 2021; Erol and François, 2018; Mehraeen et al., 2022; Rivera et al., 2016; Zhou et al., 2022), and some new BHE array models consider groundwater flow (Al-Khoury et al., 2021; Erol and François, 2018; Rivera et al., 2016; Zhou et al., 2022). Also, to consider a vertically distributed thermal conductivity of the ground, some novel thermal response test (TRT) methods were developed (Clemenzi et al., 2017; Fujii et al., 2009; Oberdorfer, 2014; Soldo et al., 2016). In summary, it follows that a comprehensive assessment of the impact of site properties on BHE performance is necessary.

The first aspect of the site characteristics comprises the thermogeological conditions, i.e. the Darcy flux, depth of groundwater table, and the geothermal gradient at the site. Dehkordi and Schincariol (2014) investigated the importance of groundwater flow and thermal

* Corresponding author at: Goldschmidtstr. 3, Göttingen 37077, Germany.
E-mail address: quan.liu@uni-goettingen.de (Q. Liu).

https://doi.org/10.1016/j.geothermics.2023.102785
Received 4 April 2023; Received in revised form 25 June 2023; Accepted 12 July 2023
Available online 22 July 2023

conductivity on the total energy extraction of a BHE system. Smith and Elmore (2018) believed that seasonal changes of the groundwater table also have a great influence on the effectiveness of the BHE. Geothermal gradient is commonly treated as a crucial influencing factor for BHE performance (Jia et al., 2021; Kurevija et al., 2011).

The site characteristics on the ground surface comprise surface temperature variation, solar irradiation, long-wave radiation, and rainfall. A Cauchy-type boundary is commonly recommended to consider heat exchange on the ground surface (Herb et al., 2008; Pollack et al., 2005), which may cause a remarkable influence on temperature evolution within the BHE array (Rivera et al., 2016). Rainfall infiltration proved to be an important factor influencing a horizontal heat exchanger GHP system (Go et al., 2015), but the impact on a vertical exchanger GHP is rarely studied.

The second aspect of the site characteristics includes thermal conductivity of the geological materials, hydraulic conductivity and heterogeneity. Luo et al. (2014) investigated BHE performance in a layered subsurface by numerical modeling, and Erol and François (2018) and Hu (2017) further developed analytical models for a multilayered aquifer. But so far, few studies have discussed the effects of a completely heterogeneous subsurface (Walker et al., 2015).

Parameter sensitivity studies can be performed to analyze the impact of site characteristics on BHE array performance. Although some of the aforementioned characteristics and properties have been investigated in relevant studies (Erol and François, 2018; Zanchini et al., 2012), it is still necessary to pay attention to all of these factors, to identify their relative importance and to assess their sensitivities and combination effects. This is especially helpful for system designers and practitioners because the mentioned site characteristics are usually difficult or expensive to be investigated and quantified. And, if the uncertainty remaining after site characterization can be evaluated, an optimized design and management of the BHE-coupled GHP system can be achieved (Monzó et al., 2016).

In this study, a BHE array is numerically simulated by coupling the Eskilson and Claesson (1988) BHE model and a heterogeneous hydrogeological model, which was developed using the FEFLOW software, version 7.5 (Diersch et al., 2010). After model validation, a sensitivity analysis considering nine site characteristics and properties is performed, based on data from a planned real geothermal site. Uncertainty issues are discussed, which may be helpful to assess impacts of site properties on design and operation of BHE arrays.

2. Governing equations of the BHE array model

Fig. 1 illustrates the heat transfer process in a BHE and influencing factors. Firstly, heat exchange between the BHE and the surrounding ground is affected by the thermogeology of the heterogeneous subsurface. Groundwater flow with a complex pattern often exists within the subsurface, which will transport heat or cold around the BHE. The groundwater table elevation may be seasonally variable, and can fluctuate within a range of several meters (Almedeij and Al-Ruwaih, 2006; Nygren et al., 2020). And, the heat extraction depends on the geothermal gradient at the site. In the shallow subsurface, the geothermal gradient may be spatially variable, depending on local geological or land use conditions. Also, the seasonally variable heat energy flux on the ground surface and rainfall when the infiltration is rapid, can influence BHE array performance as well (Vangkilde-Pedersen et al., 2012).

2.1. Heat transfer in the BHE

Heat transfer in the BHE occurs based on two mechanisms: forced convective heat transfer from the carrying fluid to the pipe wall and natural conductive heat transfer within the grout, and eventually to the surrounding ground. To describe these heat transfer mechanisms, an explicit relation of heat transfers between pipe-in, pipe-out and borehole wall was first derived by Eskilson and Claesson (1988). The heat transfer between the BHE components is assumed to correspond to a Delta configuration with three thermal resistors. By ignoring the heat capacity in the grout, a local steady-state analytical solution can be obtained. Taking a single U-pipe BHE as an example, the local steady-state heat balance equation expresses as,

$$-\rho_b c_b u(\nabla_z T_i) = \frac{T_i - T_g}{R^{\Delta}_{i-s}} + \frac{T_i - T_o}{R^{\Delta}_{i-o}} \tag{1}$$

$$\rho_b c_b u(\nabla_z T_o) = \frac{T_o - T_g}{R^{\Delta}_{o-g}} + \frac{T_o - T_i}{R^{\Delta}_{i-o}} \tag{2}$$

where ρ and c represent the density and specific heat capacity, respectively. u is the brine flow rate and T is the temperature. ∇_z is the differential operator with respect to the direction of the depth. The subscripts b, i, o, and g denote the carrying fluid (i.e., glycol mixture), pipe-in, pipe-out, and ground, respectively. R^{Δ} denotes the thermal resistance, and the subscript in R^{Δ}_{i-g} means that the active area of this thermal resistance is between pipe-in and ground. Eq. (1) implies that the heat loss in a unit length of pipe-in equals the sum of heat flux transferred from the pipe-in to ground and from the pipe-in to the pipe-out. Likewise, Eq. (2) is with respect to the heat changes in the unit length of pipe-out. The detailed derivation of these formulas and the definitions of thermal resistance is provided in e.g. Diersch et al. (2011a). The local steady-state heat balance equations can be extended to the configuration of a 2U-pipe BHE, for more details please refer to

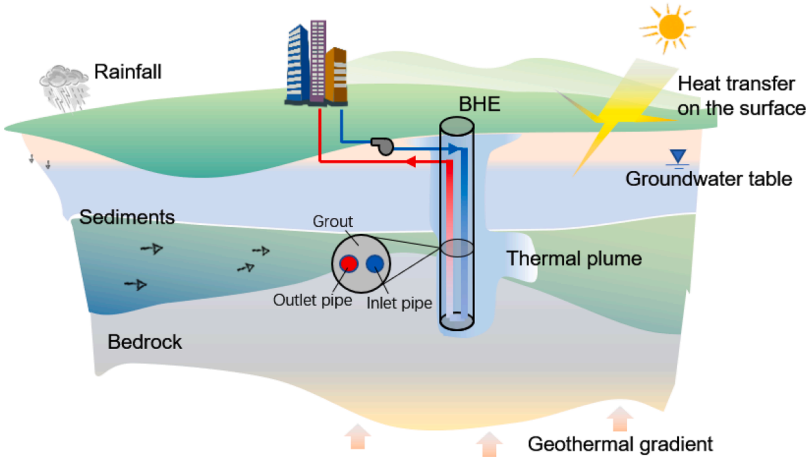

Fig. 1. Sketch of heat transfer in a BHE including influencing factors.

Diersch et al. (2010).

There are some assumptions made in the aforementioned equations. First, the transient three-dimensional (3D) heat transfer in the BHE is simplified into a quasi-3D steady-state process by ignoring the heat capacities of the BHE components. Also, the U-pipe is assumed to be arranged symmetrically within the borehole, and the vertical heat conductivity in the U-pipe is neglected. These assumptions greatly shorten the time needed to solve heat transfer problems in a large BHE array, which allows the Eskilson and Claesson (1988) model to be used for long-term simulations. It is worth noting that a constrained application time scale is required due to the steady-state assumption,

$$t > t_{limit} = \frac{5d_b^2}{4\alpha} \tag{3}$$

where d_b is the borehole diameter, and α is the thermal diffusivity of the ground. Constraint (3) indicates that the steady-state equations can be applied for transient inputs of e.g. inlet temperature, brine flow rate, or heat load only on a time scale larger than t_{limit} (generally several hours). Since the main focus of this study is to investigate the behavior of a large-scale BHE array during 1 year of operation, the Eskilson and Claesson (1988) model is suitable and efficient for the computations.

2.2. Heat transfer in the surrounding ground

For heat transfer outside the BHE, a complex theromogeology needs to be considered, which is typically a heterogeneous subsurface with flowing groundwater. The transient heat transfer equation for heterogeneous porous media is employed, given as,

$$(\rho c)_{ef}\frac{dT_s(\boldsymbol{x},t)}{dt} + \rho_w c_w v \nabla T_g(\boldsymbol{x},t) - \nabla\left(\lambda(\boldsymbol{x})_{ef}\nabla T_g(\boldsymbol{x},t)\right) = Q_T \tag{4}$$

where $T_g(\boldsymbol{x},t)$ is ground temperature depending on the spatial location $\boldsymbol{x}$ and time t. λ is thermal conductivity, which can be space-dependent considering thermal heterogeneity. Q_T denotes a thermal source or sink in the ground. The subscript w represents groundwater and ef denotes an effective parameter. The effective volumetric heat capacity and effective thermal conductivity are calculated following an arithmetic mean weighted by a porosity ε,

$$(\rho c)_{ef} = \varepsilon\rho_w c_w + (1-\varepsilon)\rho_g c_g \tag{5}$$

$$\lambda_{ef} = \varepsilon\lambda_w + (1-\varepsilon)\lambda_g \tag{6}$$

And, v in Eq. (4) denotes the Darcy flux in the aquifer. To calculate the Darcy flux, the mass conservation equation of groundwater flow is used,

$$s_s\frac{\partial h}{\partial t} + \nabla\cdot v = Q_H \tag{7}$$

where s_s is the specific storage, h is the hydraulic head, and Q_H is the hydraulic source. According to the Darcy's law, the Darcy flux in the aquifer reads as,

$$v = -k(\boldsymbol{x})\nabla h \tag{8}$$

where $k(\boldsymbol{x})$ is the space-dependent hydraulic conductivity.

2.3. Initial and boundary conditions

For heat transfer, the initial condition is set by assigning an initial temperature distribution within the whole simulation domain. In practice, the ground temperature distribution cannot be easily obtained, and is often affected by groundwater flow and thermogeology. In this study, we assumed that the undisturbed initial ground temperature profile is linear with a constant geothermal gradient (G). The initial temperature profile (T_0) along the depth (z) thus expresses as,

$$T_0(z) = T_{gs} + Gz \tag{9}$$

where T_{gs} is the temperature of the ground surface at a specified time, and can be assigned by a constant value which corresponds to the annual mean ambient temperature averaged over 20 m. Heat flux on the ground surface boundary is also considered. Heat transfer on the surface is subject to multiple thermophysical processes, such as solar radiation, precipitation-induced heat exchange, etc. (Herb et al., 2008; Wei et al., 2014; Zhou et al., 2021). To simplify these complex thermophysical processes, an effective heat transfer coefficient (I) is defined to describe the heat flux between the air at temperature T_{air} and the ground at temperature T_{gs} (Rivera et al., 2016),

$$\lambda_g\frac{\partial T_g}{\partial z}\Big|_{z=0}^{z=p} = I(\boldsymbol{x},t)\left(T_{gs} - T_{air}\right) \tag{10}$$

where λ_g is the thermal conductivity of the ground, and p is the height of the air temperature monitoring sensor which is assumed to be 3 m in the following study. It is worth noting that I does not just describe the heat exchange between the air and the ground, but represents the combined effects of all thermal processes on the ground surface as well. Considering land use and meteorological conditions, such as strong wind, short-term heavy precipitation etc., $I(\boldsymbol{x},t)$ can be variable with space and time. Although heat flux on ground surface is affected by many factors, the estimation of I for a specific site can be achieved by parameter calibration (Palmer et al., 1992; Pollack et al., 2005). In this study, we assumed that I is constant and uniform on the ground surface, focusing mainly on the influence of its magnitude. The other boundaries are assumed to be no heat flux boundaries, except for cases regarding geothermal gradient scenarios where a constant temperature boundary condition with linear variation along depth is specified.

The initial condition for groundwater flow is implemented by assigning a head H_0 on the whole domain. To consider different Darcy flux values in the aquifer, different constant heads are set on the lateral boundaries. A water-flux boundary is utilized on the ground surface to consider the recharge by rainfall,

$$k_g\frac{\partial h}{\partial z}\Big|_{z=0} = \gamma R \tag{11}$$

where k_g is hydraulic conductivity of the ground, γ is the feed coefficient of precipitation infiltration, and the R is the rainfall. A monthly average rainfall is used in the following simulations. The remaining boundaries are set as no-flow boundaries.

3. Model implementation and validation

Firstly, the Eskilson and Claesson (1988) solution Eqs. (1) and (2) is solved on 1D line elements by using the FEFLOW software's built-in BHE model. The relevant thermal resistances are calculated automatically in FEFLOW. The heat load, such as inlet temperature and fluid flow rate, can be inputted in as time series, but a time scale limitation (defined by Eq. (3)) must be satisfied. Secondly, the hydrogeothermal equations for describing heat transport and groundwater flow in the subsurface are solved in 3D by using the finite element method. Heat exchange between the BHE and the surrounding ground is achieved by assigning a Cauchy-type boundary condition that couples the temperature and heat flux on the borehole wall.

To improve the reliability during the numerical calculation and to consider the borehole radius in the simulations, a specific mesh is adopted. An ideal element size around the BHE node is assigned by adjusting the distance to the surrounding secondary nodes. The formula for calculating the distances between was addressed by Diersch et al. (2011b). In this study, six extra nodes are added around each BHE node, and the distance between the extra node and the BHE node is set to 0.46 m.

Afterwards, the BHE array model established in FEFLOW is validated. The model setup and the validation results are shown in Fig. 2. The outlet temperature changes calculated by the steady-state (Eskilson and Claesson, 1988) BHE model are firstly verified by comparing to the results of the fully transient BHE model in FEFLOW (Diersch et al., 2011a). These two simulations are both based on the model setup shown in Fig. 2a. A double U-pipe is employed with an inlet temperature of 30 °C and a flow rate of 20 m^3/d. The initial ground temperature is 10 °C. Comparing the two curves in Fig. 2b, it was found that the difference of the outlet temperature simulated by the Eskilson & Claesson (1988) model and by the fully transient model is evident at early time, and becomes very small (ca. 0.48 °C) when the time is close to t_{limit}. This reflects that the Eskilson & Claesson (1988) solution is reliable when the heat load varies at a time scale larger than t_{limit}. The small difference may be due to the fact that the analytical solution ignores the vertical heat conductivity in the pipes. Secondly, the ground temperature simulated by FEFLOW is verified by comparing with the results of the line source analytical model (Al-Khoury et al., 2021; Molina-Giraldo et al., 2011) and of a model developed using COMSOL software (Multiphysics, 2012). The simulations are based on the model setup shown in Fig. 2a and the double U-pipe BHE is replaced by a line source model because few analytical models can consider the heat transfer both in the actual BHE and in the surrounding ground. The line source has a length of 50 m and with a heat transfer rate of 20 W/m. To test the FEFLOW model in dealing with multiple line sources, five line sources arranged in a row and nine line sources arranged arbitrarily are both considered. All simulated ground temperature distributions at a depth of 30 m are plotted in Fig. 2c. By comparison, it can be seen that the contour lines simulated by the different solutions for 10 years are very close although the line sources are arranged in different patterns.

4. Sensitivity analysis

4.1. Base case scenario

To investigate the sensitivity of the BHE array performance under different site characteristics, a geothermal heat pump (GHP) system planned to be installed at a site located in the city of Hannover in Germany was selected to provide data. Although the project is still in the design phase, the heat load of the BHE system can be simulated based on the expected heating and cooling demands, aiming at investigating sensitivity of characteristic site parameters. The BHE array consists of 96 BHEs which are installed in a rectangular grid with 6 rows and 16 columns. The length of each BHE is 150 m and the BHE spacing is 8 m. The carrying fluid is injected in a parallel mode. The detailed parameters of the BHE design are listed in Table 1. According to the regional geological background, the stratigraphic lithology at this site is composed of strongly weathered limestone. Due to the current lack of detailed information about the underground thermogeology at this site, some assumptions were made in assigning the modeling parameters (see Table 1). For instance, the initial temperature is assumed to be uniformly 12.1 °C, and the Darcy flux in the aquifer is fixed to 0.0864 m/d. Additionally, some other parameters are idealized in the base case. The vadose zone is neglected, and the groundwater flow in the aquifer is considered homogeneous. The complicated heat and mass transport processes at the ground surface and a geothermal gradient within the subsurface are not considered. Nevertheless, the uncertainty caused by these assumptions will be discussed in the following sensitivity analysis.

Firstly, some time series are assumed during the 1st year operation, including the flow rate of the working fluid, inlet temperature, and air

Table 1
Parameter settings of the base case scenario.

Parameter	Value
Geometrical parameters	
Depth of borehole L (m)	150
Borehole diameter d_b (m)	0.15
Borehole spacing s_b (m)	8
Outer diameter of pipe-out or pipe-in d_p (m)	0.032
Shank spacing of the double-U pipe s_p (m)	0.08
Pipe wall thickness d_w (m)	0.0029
Hydrogeological and geothermal parameters	
Initial temperature T_0 (°C)	12.1
Thermal conductivity of grout λ_g $(W/m/K)$	1.2
Thermal conductivity of fluid in the U-pipe λ_b $(W/m/K)$	0.6
Heat capacity of fluid c_b $(kJ/m^3/K)$	4175
Density of fluid ρ_b (kg/m^3)	1000
Thermal conductivity of ground λ_s $(W/m/K)$	2
Heat capacity of ground c_s $(kJ/m^3/K)$	2300
Density of ground ρ_s (kg/m^3)	1650
Darcy flux in the aquifer u (m/d)	0.0864

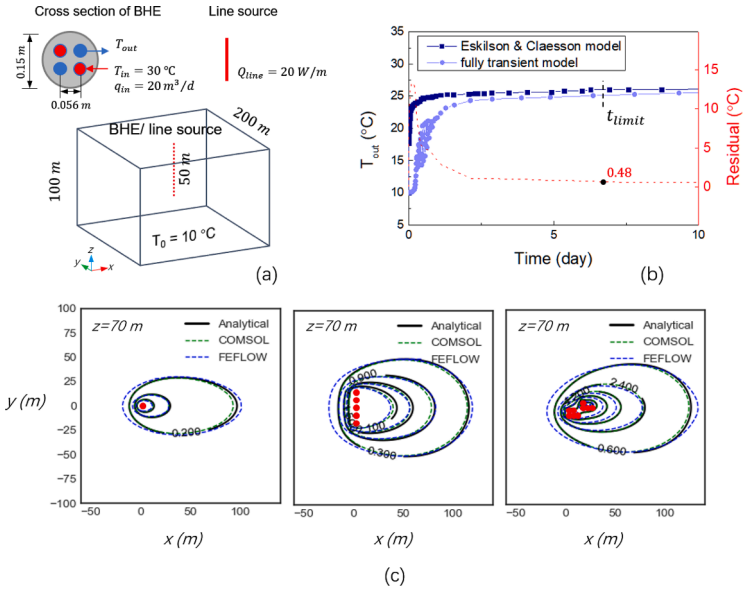

Fig. 2. (a) The setup for model validation. The comparison of (b) BHE outlet temperatures simulated by the Eskilson & Claesson (1988) model and by the fully transient model, and the residual between them. (c) The contour lines of ground temperature at a depth of 30 m calculated by the line source analytical model and the COMSOL model. The red points represent the line source locations.

temperature. The heat loads, i.e. fluid flow rate and inlet temperature, are simulated using the TRNSYS software (www.tess-inc.com) to consider the heat transfer process in buildings and GHP under the expected heating and cooling demands, in which photovoltaic-thermal collectors are integrated with the GHP system. According to the aforementioned assumptions, the *Baseline Case* conceptual model and the simulated time series at the site are plotted in Fig. 3. The size of the numerical FEFLOW model is 400 m (length) × 150 m (width) × 200 m (depth). The heat loads will be specified as inputs to the FEFLOW model, and the air temperature will be considered in scenarios where the ground surface based thermal effect is significant.

After running the simulation for one year, the results are shown in Fig. 4. Temperature evolution in the subsurface at 150 days and 300 days is plotted in Fig. 4a and 4b, respectively. A thermal drift is observed due to the groundwater flow. Since in the model the subsurface is considered homogeneous and the hydrologic conditions constant, including the Darcy flux, the temperature isosurface is moving gradually to the right side. In Fig. 4c, the simulated outlet temperatures of the 96 BHEs are depicted. A small difference between the temperatures is observed, especially in summer. This is because of the groundwater flow and the strong fluctuation of the inlet temperature leads to a difference in energy extraction between the BHEs located upstream and downstream. Finally, to quantify the BHE array performance, a parameter describing total heat production $THP(t)$ is introduced, which is given as,

$$THP(t) = \int_0^t \sum_{m=1}^{96} \left(T_o^m - T_i\right) q_{in} \rho_b c_b dt \tag{12}$$

where m is the number of the BHEs, and T_o and T_i represent the time series of simulated BHE outlet temperature and assigned inlet temperature, respectively. $THP(t)$ is the accumulated heat production during a period of service time t. THP can be viewed as an indicator to evaluate the BHEs performance (Tang and Nowamooz, 2019). The simulated THP in the base case scenario is shown in Fig. 4d. The THP curve during the 1-year simulation can be divided into three periods, heat extraction (< 120 days), heat injection (120 days ~ 270 days), and heat extraction (> 270 days). After the first heat extraction-injection cycle, the THP is close to zero. It implies that a heat balance is achieved at this site under the current scenario settings. The maximum heat production is about 340 MWh, and the annual THP is 221.2 MWh.

4.2. Investigated factors

Subject to the field conditions or available financial budget, site characteristics usually cannot be adequately investigated which may cause an uncertainty in the prediction of BHE array performance. To study the sensitivity, nine factors were selected with respect to the site characteristics.

(1) *Darcy flux in the aquifer*

It is well known that flowing groundwater plays an important role in heat transfer in the subsurface. The higher the groundwater flow velocity is, the faster could be the heat convection. Darcy flux in the aquifer is thus treated as a sensitivity factor to study the effect on heat production. Four Darcy flux values were considered in this study: 1×10^{-8}, 1×10^{-7}, 1×10^{-6}, and 1×10^{-5} m/s.

(2) *Thermal conductivity and volumetric heat capacity of the ground*

For a shallow BHE system, thermal conductivity of geologic materials underground is another important factor that affects the heat conduction process between the BHE and the surrounding ground. In general, thermal conductivity varies from 0.4 to 4.2 W/m/K (Stylianou et al., 2016). Levels of 1, 2, 3, and 4 W/m/K were selected in the sensitivity analysis. Changes in the volumetric heat capacity are known to have only a limited impact on the long-term heat production (Oberdorfer, 2014; Tang and Nowamooz, 2019). To confirm this, we performed some additional simulations based on the *Baseline Case*, using values of 1.8, 2.8, 3.8 and 4.8 MJ/m^3/K.

(3) *The depth of groundwater table*

The groundwater table can be considered a boundary between heat conduction and conduction-advection modes in the subsurface. Clearly, heat exchange in the vadose zone is merely through the conductive mode, and both conductive and convective modes need to be considered in the aquifer. Affected by regional boundary conditions, groundwater depth may significantly vary seasonally. In this study, four groundwater depths of 0 m, 10 m, 25 m and 50 m were investigated.

(4) *Hydraulic and thermal heterogeneity of the subsurface*

To consider heterogeneous subsurface media, four degrees of heterogeneity were employed for hydraulic conductivity (k) and thermal conductivity of the ground (λ), respectively. For the *Baseline case*, the subsurface is considered homogeneous (i.e. $log_{10}(k)$ is fixed to −4.5 and λ is set to 2 W/m/K). In *Case 1*, a three-layered subsurface is explored, and the thermogeological parameters are uniform in each layer, where $log_{10}(k)$ of the upper, middle, and bottom layers are −5.5, −4.5, and −5.25. Also, the thermal conductivity of the three layers are 1.25, 1.5, and 2.8 W/m/K, respectively. The parameters of each layer are oriented on the values in the *Baseline Case* to make the simulation results comparable. From *Case 2* to *Case 3*, two geostatistical distributions were

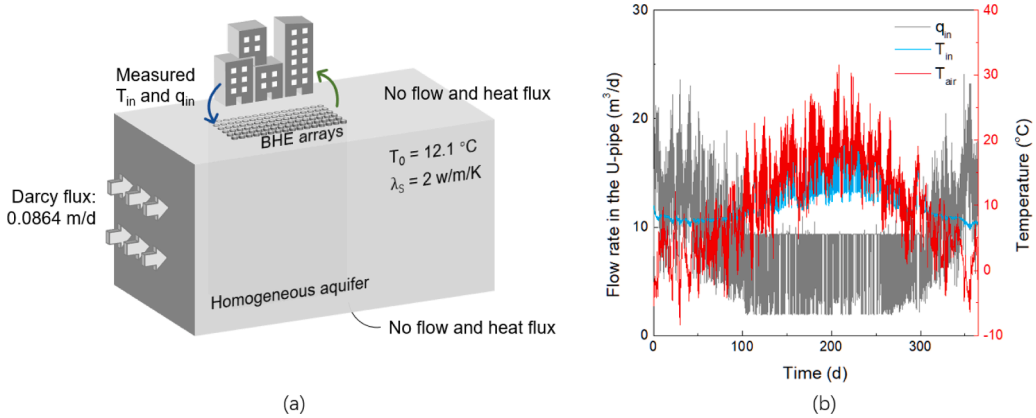

Fig. 3. (a) Conceptual model of the base case scenario, and (b) the simulated time series of flow rate in the U-pipe q_{in}, inlet temperature T_{in}, and the air temperature T_{air} when operating the BHEs.

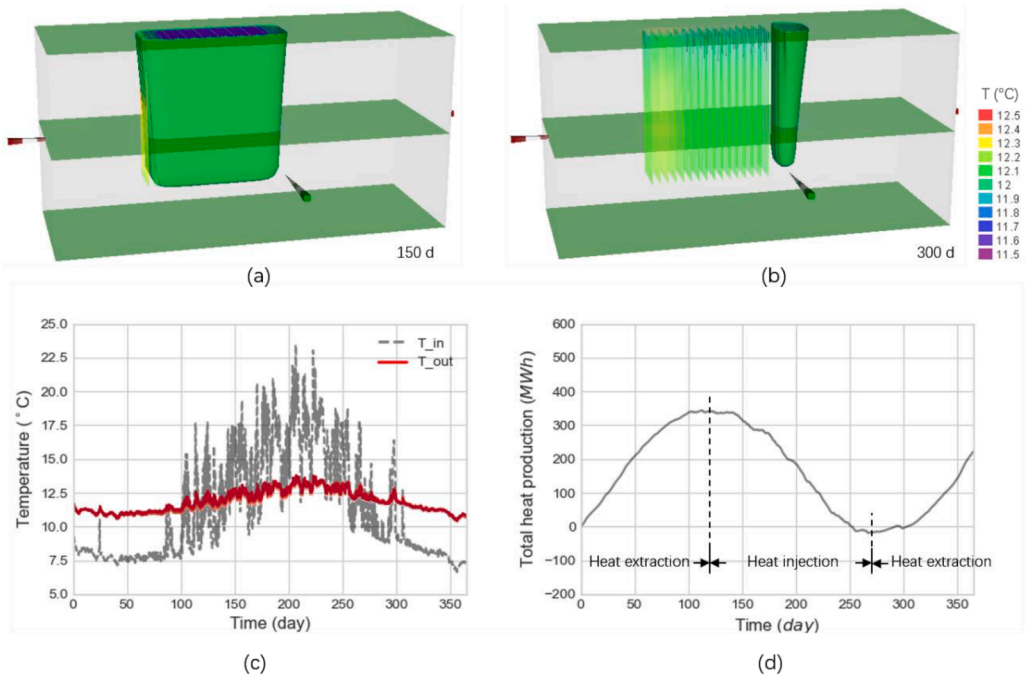

Fig. 4. Simulation results of the base case scenario for the temperature evolution in the subsurface at (a) 150 days and (b) 300 days. The simulated outlet temperature time series bandwidth of the 96 BHEs (red lines) is shown in (c), and total heat production curve during the 1 year simulation shown in (d).

assigned for $log_{10}(k)$ and λ. They were generated by the anisotropic Gaussian model. An independent variogram function was assigned for each layer and a relatively shorter range was assigned to the depth direction. Considering a possible inclination of layers, different dips and strikes were set for the three layers. The anisotropic ranges (I) and the orientation ($dip,\ strike$) of the three layers are,

$$I|_{up} = [50,\ 50,\ 5],\ [dip,\ strike]|_{up} = [-60,\ 40],$$

$$I|_{mid} = [50,\ 50,\ 5],\ [dip,\ strike]|_{mid} = [-10,\ 80],$$

$$I|_{bot} = [50,\ 50,\ 20],\ [dip,\ strike]|_{bot} = [80,\ 120],$$

where the subscripts *up*, *mid*, and *bot* represent the upper layer, middle layer and bottom layers, respectively. The orientation angle is clockwise from the positive x direction. Fig. 5 shows the distributions of $log_{10}(k)$ and thermal conductivity within the three layers. In both *Case 2* and *Case 3*, the variogram functions have the nugget (N) values,

$$N|^{H}_{up} = -5.5,\ N|^{T}_{up} = 1.25,$$

$$N|^{H}_{mid} = -4.5,\ N|^{T}_{mid} = 1.5,$$

$$N|^{H}_{bot} = -5.25,\ N|^{T}_{bot} = 2.8,$$

where the superscripts of H and T represent $log_{10}(k)$ and thermal conductivity, respectively. The only difference between *Case 2* and *Case 3* is with respect to the scale (or partial sill) values in the variogram functions. The scale values (S) for these two levels are set as,

$$S|^{H}_{up} = [1,\ 2],\ S|^{T}_{up} = [0.25,\ 0.5],$$

$$S|^{H}_{mid} = [1.5,\ 2.5],\ S|^{T}_{mid} = [0.5,\ 0.75],$$

$$S|^{H}_{bot} = [0.75, 1.75],\ S|^{T}_{bot} = [0.4, 0.8].$$

The first value in the brackets is for *Case 2* and the second one is for *Case 3*. This indicates that *Case 3* is more heterogeneous compared to *Case 2*.

(5) *Initial geothermal gradient*

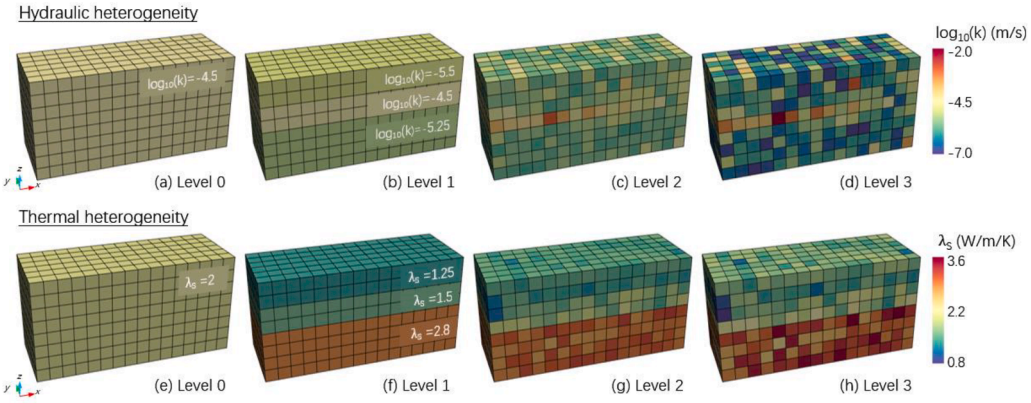

Fig. 5. $log_{10}(k)$ of the hydraulic conductivity (k) and thermal conductivity (λ) distributions with four degrees of heterogeneity.

The initial ground temperature profile is generally site-dependent, and is affected by many factors, such as the regional hydrogeological conditions and the air temperature fluctuation (Saar, 2011). In this study, the initial ground temperature profile is assumed to be linear and increasing with depth. According to Eq. (9), the initial ground temperature profile can be calculated based on the air temperature (12.1 °C) and the geothermal gradient. Four geothermal gradients of −0.01, 0, 0.01, and 0.02 °C/m were selected for the sensitivity analysis. A negative geothermal gradient is considered here to account for complex hydrogeothermal conditions in the shallow subsurface, such as low-temperature horizontal flow and local incomplete heat balance (Saar, 2011).

(6) *Effective heat transfer coefficient on the ground surface*

The ground surface temperature is an important boundary condition in simulating the heat transfer. The exact ground surface temperature is generally not easy to determine and impacted by many factors. Therefore, according to the definition in Eq. (10), an effective heat transfer coefficient (I) is introduced to represent the complex heat flux at the ground surface. The value of I is found to vary within a wide range from 0.08 to 3.2 W/m^2/K (Güven et al., 1983; Palmer et al., 1992; Rivera et al., 2016). Here, four effective heat transfer coefficients were selected (i.e., 0, 2, 4, and 6 W/m^2/K, respectively).

(7) *Seasonal rainfall*

In this study, the impact of rainfall is considered as recharging aquifers in the subsurface. The rainwater temperature is assumed to be similar with the ground surface temperature which is calculated by Eq. (10). This assumption is made because temperature measurements of rainwater are generally not available. Considering the monthly rainfall history in the City of Hannover, the months of June and July are chosen as the rainy season to investigate the sensitivity of rainfall factors. The monthly rainfall in June and July varies from 10 s mm to >100 mm. Accordingly, three levels of monthly average rainfall of 50, 100, and 150 mm were assigned for June and July. Fig. 6 shows the monthly average rainfall in the 1-year simulation. A simulation of the base case without factoring in the rainfall effect is also included for comparison.

In summary, all investigated factors respective parameters and their values are summarized in Table 2.

4.3. Sensitivity of the annual heat production

The annual heat production is treated as the sensitivity indicator of the BHEs performance, which is calculated by Eq. (12) for 1 year. The annual heat production in regards with the investigated parameters is plotted in Fig. 7. The light blue circle in each graph represents the annual heat production of the *Baseline Case*. The sensitivity with respect to the Darcy flux is illustrated in Fig. 7a. When the Darcy flux is greater than 1×10^{-7} m/s, a linear relationship between the annual heat production and the log-scale Darcy flux arises. A 70 MWh heat production increase is observed for an order of magnitude increase of Darcy flux. This implies that groundwater flow has a significant, positive impact on the heat production. Fig. 7b shows a very small positive effect of the thermal conductivity of the ground as well. A 1 W/m/K increase in thermal conductivity results in a slight increase in heat production (approximately 4 MWh). This result may be countered by the specified high Darcy flux (1×10^{-6} m/s) because the influence of heat conduction will be covered by the convection process due to groundwater flow. In Fig. 7c, the sensitivity with respect to groundwater depth reflects a balance between the heat conduction and heat convection mode. With a deeper groundwater table, less heat can be transported by convection. Also shown in Fig. 7c, with an increase of groundwater table depth, the annual heat production decreases gradually (approximately 6 MWh for every 10 m rise), which implies that in the process of a declining groundwater table, heat production through conduction cannot be offset by that from convection due to groundwater flow. In other words, at this site, heat convection contributes more than heat conduction, with Darcy flux of 1×10^{-6} m/s.

The influence of thermal and hydraulic heterogeneity of the subsurface is illustrated in Figs. 7d and 7e, respectively. In Fig. 7d, the annual heat production fluctuates within 2 MWh, with the increase of thermal heterogeneity. With the increase in hydraulic heterogeneity shown in Fig. 7e, an noticeable decrease in annual heat production occurs from *Baseline Case* to *Case 1*. A 50 MWh decrease in annual heat production is observed. It indicates that a thorough investigation of the hydraulic properties is necessary to improve the prediction of the BHEs performance. It is worth noting, that a more detailed and accurate investigation of hydraulic properties does not necessarily lead to a decrease of heat production.

Fig. 7f shows the effects of the geothermal gradient on the annual heat production. A significant increase in annual heat production of about 150 MWh is modeled for every 0.01 °C/m increase of the geothermal gradient. A larger geothermal gradient corresponds with

Table 2
Summary of the parameters used in the modeling.

No.	Parameter	Levels
1	Darcy flux in the aquifer (m/s)	[1e-8, 1e-7, 1e-6*, 1e-5]
2	Thermal conductivity of ground ($W/m/K$)	[1, 2*, 3, 4]
3	Volumetric heat capacity of ground ($MJ/m^3/K$)	[1.8, 2.8*, 3.8, 4.8]
4	Depth of groundwater table (m)	[0*, 10, 25, 50]
5	Thermal heterogeneity degree	[0*, 1, 2, 3]
6	Hydraulic heterogeneity degree	[0*, 1, 2, 3]
7	Geothermal gradient (°C/m)	[−0.01, 0*, 0.01, 0.02]
8	Heat transfer coefficient on ground surface ($W/m^2/K$)	[0*, 2, 4, 6]
9	Seasonal rainfall in June and July ($mm/month$)	[0*, 50, 100, 150]

* represents the value for the *Baseline Case*.

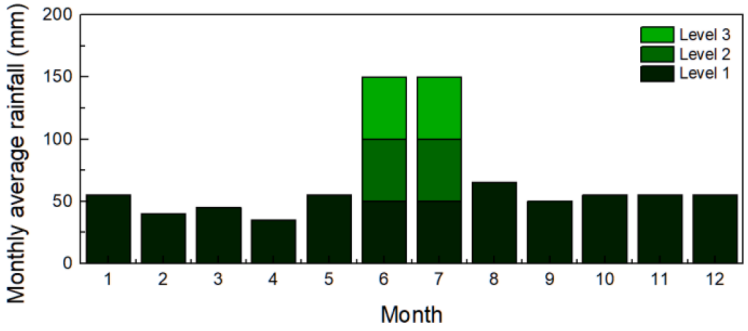

Fig. 6. Histogram of the monthly average rainfall used in the sensitivity analysis. June and July are selected for variations of the recharge, and three rainfall levels are considered.

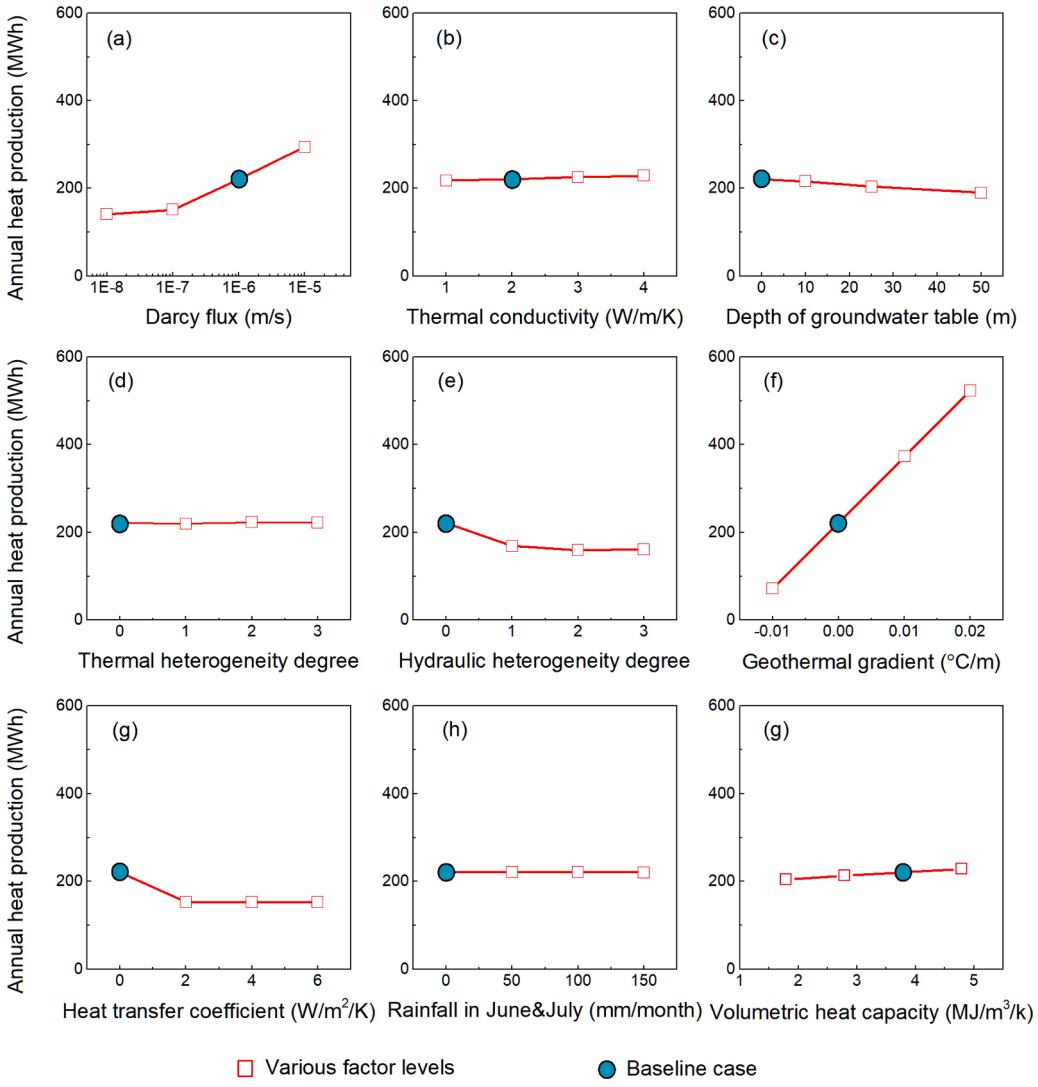

Fig. 7. Sensitivity of the annual heat production with respect to the nine parameters.

higher temperatures with depth, resulting in more energy extracted.

Figs. 7g and 7h illustrate the influence of the thermogeology on the upper boundary of the model. Both the effective heat transfer and the seasonal rainfall in June and July impact the geothermal gradient. These two scenarios represent thermal flux and mass flux conditions. The influence of the effective heat transfer coefficient is evident from Fig. 7g. With an increase of the effective heat transfer coefficient, the annual heat production first drops significantly (approximately 68 MWh), and stabilizes gradually. This indicates that BHEs may be able to extract more heat when the effective heat transfer coefficient is small. As this coefficient increases, more shallow ground heat will be exchanged with the atmosphere, resulting in less heat production by the BHEs. In the example shown, once the effective heat transfer coefficient is greater than 2 W/m^2/K, its influence on the heat production is small, and heat flux on the ground surface is no longer an evident impact on the heat production, which will be mainly governed by the thermal conductivity. As Fig. 7h shows the influence of seasonal rainfall is relatively small. The annual heat production varies less than 1 MWh, which is observed with increasing rainfall.

5. Discussion

5.1. Dimensionless Peclet number

To assess the combined effects of heat conduction and heat convection in the subsurface on the BHE array behavior, a dimensionless *Peclet* number is introduced. It is defined as the ratio of advective heat transport by groundwater flow to conductive heat transport by the ground (Molina-Giraldo et al., 2011),

$$Pe = \sum_{1}^{n} \frac{\rho_w c_w v L_j}{\lambda_s} \tag{12}$$

where L_j represents the length of a depth interval j with constant thermogeology. For instance, when considering the depth of the groundwater, the *Peclet* number can be regarded as a weighted sum with respect to the vadose zone thickness and aquifer thickness. In this sensitivity analysis, various values for the Darcy flux, thermal conductivity of the ground, depth of the groundwater table, and heterogeneity degree (*Baseline Case*) are considered, and, by using the *Peclet* number, their joint effects on the annual heat production can thus be evaluated.

The relation between the *Peclet* number and the annual heat production is depicted in Fig. 8. A total of 64 crossover scenarios with a varying Darcy flux (1×10^{-8}, 1×10^{-7}, 1×10^{-6} and 1×10^{-5} m/s),

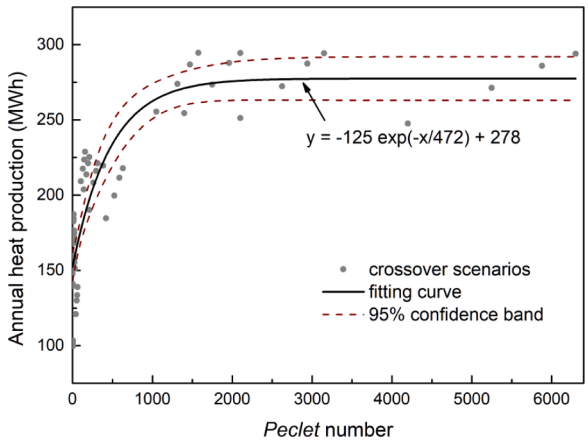

Fig. 8. Regression analysis of the relationship between the Peclet number and annual heat production.

thermal conductivity of the ground (1, 2, 3, and 4 W/m/K), and groundwater level (0, 10, 25, and 50 m) were considered. The regression curve of all the simulation results and its 95% confidence interval are shown as well in Fig. 8. The slope of the regression curve indicates that the annual heat production is mainly sensitive to the *Peclet* number when less than 1000. When the *Peclet* number is small (<20), which means heat transfer in the subsurface is dominated by conduction, the annual heat production varies around 153 MWh. If heat transfer in the subsurface is dominated by convection (i.e. the *Peclet* number is above 1500), the annual heat production stabilizes at around 278 MWh. The regression curve implies that the uncertainty of annual heat production from the site characteristics is about 125 MWh. Furthermore, it is worth noting that the geothermal gradient is constant for these crossover scenarios and the rainfall and heat exchange with atmosphere on the ground surface is not considered by the *Peclet* number.

5.2. Space-time variation of the investigated factors

In the sensitivity study, some parameters were assumed to be time-independent, such as the Darcy flux, groundwater depth, and the effective heat transfer coefficient. In fact, the Darcy flux in the aquifer could be dynamic and influenced by the regionally fluctuating hydraulic gradient and rainfall. Heat convection induced by the Darcy flux occurs only in the subsurface under the groundwater table. Additionally, the effective heat transfer coefficient describing the heat flux on the ground surface is kept constant throughout the whole simulation period and imposed uniformly. However, the heat flux on the ground surface is space-time dependent in reality. Different ground surfaces, such as pavement, buildings or grassland, have significantly different thermal properties. Moreover, the initial ground temperature was assumed to be linearly distributed in all simulations. Finally, short-term heavy precipitation could be an important factor affecting the heat flux on the ground surface (Wei et al., 2014). Therefore, the effects of the space-time variation of the above-mentioned factors need to be further studied.

6. Summary

To assess the influence of site characteristics on the performance of BHEs, a numerical model was developed. Given a long-term simulation and a large-scale BHE array, a local steady-state analytical BHE model was employed. This analytical model was coupled with a 3D numerical ground-aquifer model to simulate the impacts of groundwater flow, subsurface heterogeneity and various boundary conditions. After model validation, nine parameters were evaluated, including Darcy flux in the aquifer, thermal conductivity and volumetric heat capacity of the ground, groundwater depth, thermogeological heterogeneity, geothermal gradient, heat transfer coefficient on the ground surface, and seasonal rainfall. According to the sensitivity analysis of the considered *Baseline Case*, we can conclude the following:

(1) The geothermal gradient has the most significant impact on the annual heat production. Considering a Darcy flux of 1×10^{-6} m/s, a significant increase of about 150 MWh of annual heat production is observed for every 0.01 °C/m increase of the geothermal gradient. The second sensitivity factor is the Darcy flux ($> 1 \times 10^{-7}$ m/s) in the aquifer. A 70 MWh heat production increase results from an order of magnitude increase of the Darcy flux. Together with the thermal conductivity and volumetric heat capacity of ground, the increase of these three parameters have positive effects on the annual heat production.
(2) The increase of the groundwater table depth and increase of the heat transfer coefficient on the ground surface lead to a decrease in the annual heat production. A drop in the groundwater table leads to a linear, small decrease (approximately 6 MWh for every 10 m depth) of annual heat production, and the heat transfer coefficient results in a decrease of 68 MWh annual heat production, when the coefficient varies between 0 and 2 W/m^2/K.
(3) The variations in the ground thermal heterogeneity and seasonal rainfall intensity (only mass recharge considered) have little impacts on the annual heat production, which varies within 2 MWh.
(4) Change in the hydraulic heterogeneity is an important factor influencing the annual heat production. A detailed investigation of hydraulic properties is helpful for improving the prediction of BHEs performance.

A *Peclet* number is adopted to assess the combined effects of Darcy flux, thermal conductivity of the ground and groundwater depth. A regression analysis of the relationship between the *Peclet* number and the annual heat production provides an assessment of uncertainty of heat production due to these related factors. Compared to thermal conductivity of the ground and groundwater depth, the Darcy flux has a larger variability, which may introduce higher uncertainty in heat production of the BHE arrays. Therefore, an evaluation of these parameter can lead to a more reliable quantification. Up to now, the impacts of space-time variation have not been included in the sensitivity analysis, which offers the chance for further studies. In a next step, we would also like to focus on the global sensitivity of the long-term performance of BHE systems to site characteristics.

Declaration of Competing Interest

The authors declare that they have no known competing financial interests or personal relationships that could have appeared to influence the work reported in this paper.

Data availability

Data will be made available on request.

Acknowledgements

This work was financed by the German Ministry for Economic Affairs and Climate Action, grant No. 03EE4021B. We thank the colleagues from the Institute for Solar Energy Research in Hameln and from the LBEG in Hannover for fruitful discussions and data sharing.

References

Al-Khoury, R., BniLam, N., Arzanfudi, M.M., Saeid, S., 2021. Analytical model for arbitrarily configured neighboring shallow geothermal installations in the presence of groundwater flow. Geothermics 93, 102063.

Almedeij, J., Al-Ruwaih, F., 2006. Periodic behavior of groundwater level fluctuations in residential areas. J. Hydrol. 328 (3-4), 677–684.

Bassetti, S., Rohner, E., Signorelli, S., Matthey, B., 2006. Dokumentation von Schadensfällen bei Erdwärmesonden. Geowatt AG. Schlussbericht.

Clemenzi, R., Ewbank, G., Siglin, J., Liu, X., 2017. Thermal Response Testing Takes a Step Forward. Geo Outlook 14 (3).

Dehkordi, S.E., Schincariol, R.A., 2014. Effect of thermal-hydrogeological and borehole heat exchanger properties on performance and impact of vertical closed-loop geothermal heat pump systems. Hydrol. J. 22 (1), 189–203.

Diersch, H.J., Bauer, D., Heidemann, W., Rühaak, W., Schätzl, P., 2011a. Finite element modeling of borehole heat exchanger systems: Part 1. Fundamentals. Comput. Geosci. 37 (8), 1122–1135.

Diersch, H.J., Bauer, D., Heidemann, W., Rühaak, W., Schätzl, P., 2011b. Finite element modeling of borehole heat exchanger systems: Part 2. Numerical simulation. Comput. Geosci. 37 (8), 1136–1147.

Diersch, H., Bauer, D., Heidemann, W., Rühaak, W., Schätzl, P., 2010. Finite element formulation for borehole heat exchangers in modeling geothermal heating systems by FEFLOW. WASY Software FEFLOW White Paper 5, 5–96.

Erol, S., François, B, 2018. Multilayer analytical model for vertical ground heat exchanger with groundwater flow. Geothermics 71, 294–305.

Eskilson, P., Claesson, J., 1988. Simulation model for thermally interacting heat extraction boreholes. Numer. Heat Trans. 13 (2), 149–165.

Florea, L.J., Hart, D., Tinjum, J., Choi, C., 2017. Potential impacts to groundwater from ground-coupled geothermal heat pumps in district scale. Groundwater 55 (1), 8–9.

Fujii, H., Okubo, H., Nishi, K., Itoi, R., Ohyama, K., Shibata, K., 2009. An improved thermal response test for U-tube ground heat exchanger based on optical fiber thermometers. Geothermics 38 (4), 399–406.

Go, G.H., Lee, S.R., Nikhil, N., Yoon, S., 2015. A new performance evaluation algorithm for horizontal GCHPs (ground coupled heat pump systems) that considers rainfall infiltration. Energy 83, 766–777.

Güven, O., Melville, J., Molz, F., 1983. An analysis of the effect of surface heat exchange on the thermal behavior of an idealized aquifer thermal energy storage system. Water Resour. Res. 19 (3), 860–864.

Hein, P., Kolditz, O., Görke, U.J., Bucher, A., Shao, H., 2016. A numerical study on the sustainability and efficiency of borehole heat exchanger coupled ground source heat pump systems. Appl. Therm. Eng. 100, 421–433.

Herb, W.R., Janke, B., Mohseni, O., Stefan, H.G., 2008. Ground surface temperature simulation for different land covers. J. Hydrol. 356 (3-4), 327–343.

Hu, J., 2017. An improved analytical model for vertical borehole ground heat exchanger with multiple-layer substrates and groundwater flow. Appl. Energy 202, 537–549.

Jia, G., Ma, Z., Xia, Z., Wang, J., Zhang, Y., Jin, L., 2021. Investigation of the horizontally-butted borehole heat exchanger based on a semi-analytical method considering groundwater seepage and geothermal gradient. Renewable Energy 171, 447–461.

Kurevija, T., Vulin, D., Krapec, V., 2011. Influence of undisturbed ground temperature and geothermal gradient on the sizing of borehole heat exchangers. In: Paper presented at the Proceedings of the World Renewable Energy Congress, Linkoping, Sweden.

Luo, J., Rohn, J., Bayer, M., Priess, A., Xiang, W., 2014. Analysis on performance of borehole heat exchanger in a layered subsurface. Appl. Energy 123, 55–65.

Mehraeen, N., Ahmadi, M.M., Ghasemi-Fare, O., 2022. Numerical modeling of mixed convection near a vertical heat source in saturated granular soils. Geothermics 106, 102566.

Molina-Giraldo, N., Blum, P., Zhu, K., Bayer, P., Fang, Z., 2011. A moving finite line source model to simulate borehole heat exchangers with groundwater advection. Int. J. Therm. Sci. 50 (12), 2506–2513.

Monzó, P., Bernier, M., Acuña, J., Mogensen, P., 2016. A monthly based bore field sizing methodology with applications to optimum borehole spacing. ASHRAE Trans. 122 (1), 111–126.

Multiphysics, C., 2012. Comsol Multiphysics User Guide (version 4.3 a), p. 39. COMSOL, AB.

Nygren, M., Giese, M., Kløve, B., Haaf, E., Rossi, P.M., Barthel, R., 2020. Changes in seasonality of groundwater level fluctuations in a temperate-cold climate transition zone. J Hydrol X 8, 100062.

Oberdorfer, P., 2014. Heat Transport Phenomena in Shallow Geothermal Boreholes: Development of a Numerical Model and a Novel Extension For the Thermal Response Test Method By Applying Oscillating Excitations. Georg-August Universität, Göttingen.

Palmer, C.D., Blowes, D.W., Frind, E.O., Molson, J.W., 1992. Thermal energy storage in an unconfined aquifer: 1. Field injection experiment. Water Resour. Res. 28 (10), 2845–2856.

Pärisch, P., Mercker, O., Oberdorfer, P., Bertram, E., Tepe, R., Rockendorf, G., 2015. Short-term experiments with borehole heat exchangers and model validation in TRNSYS. Renewable Energy 74, 471–477.

Pollack, H.N., Smerdon, J.E., Van Keken, P.E., 2005. Variable seasonal coupling between air and ground temperatures: A simple representation in terms of subsurface thermal diffusivity. Geophys. Res. Lett. (15), 32.

Rivera, J.A., Blum, P., Bayer, P., 2016. A finite line source model with Cauchy-type top boundary conditions for simulating near surface effects on borehole heat exchangers. Energy 98, 50–63.

Rybach, L., Eugster, W., 2002. Sustainability aspects of geothermal heat pumps. In: Paper presented at the 27th Workshop on Geothermal Reservoir Engineering.

Saar, M.O., 2011. Geothermal heat as a tracer of large-scale groundwater flow and as a means to determine permeability fields. Hydrol. J. 19 (1), 31–52.

Schincariol, R.A., Raymond, J., 2021. Borehole Heat Exchangers—Addressing the Application Gap with Groundwater Science. Groundwater.

Signorelli, S., Kohl, T., Rybach, L., 2004. Sustainability of production from borehole heat exchanger fields. In: Paper presented at the 29th Workshop on geothermal reservoir engineering.

Smith, D.C., Elmore, A.C., 2018. The observed effects of changes in groundwater flow on a borehole heat exchanger of a large scale ground coupled heat pump system. Geothermics 74, 240–246.

Soldo, V., Boban, L., Borović, S., 2016. Vertical distribution of shallow ground thermal properties in different geological settings in Croatia. Renewable Energy 99, 1202–1212.

Stauffer, F., Bayer, P., Blum, P., Giraldo, N.M., Kinzelbach, W., 2013. Thermal Use of Shallow Groundwater. CRC Press.

Stylianou, I.I., Tassou, S., Christodoulides, P., Panayides, I., Florides, G., 2016. Measurement and analysis of thermal properties of rocks for the compilation of geothermal maps of Cyprus. Renewable Energy 88, 418–429.

Tang, F., Nowamooz, H., 2019. Factors influencing the performance of shallow Borehole Heat Exchanger. Energy Convers. Manage. 181, 571–583.

Vangkilde-Pedersen, T., Ditlefsen, C., Højberg, A.L., 2012. Shallow geothermal energy in Denmark. GEUS Bulletin 26, 37–40.

Walker, M.D., Meyer, L.L., Tinjum, J.M., Hart, D.J., 2015. Thermal property measurements of stratigraphic units with modeled implications for expected performance of vertical ground source heat pumps. Geotech. Geol. Eng. 33, 223–238.

Wei, N., Dai, Y., Zhang, M., Zhou, L., Ji, D., Zhu, S., Wang, L., 2014. Impact of precipitation-induced sensible heat on the simulation of land-surface air temperature. J. Adv. Model. Earth Syst. 6 (4), 1311–1320.

Zanchini, E., Lazzari, S., Priarone, A., 2012. Long-term performance of large borehole heat exchanger fields with unbalanced seasonal loads and groundwater flow. Energy 38 (1), 66–77.

Zhou, Y., Wu, Z.H., Wang, K., 2021. An analytical model for heat transfer outside a single borehole heat exchanger considering convection at ground surface and advection of vertical water flow. Renewable Energy 172, 1046–1062.

Zhou, Y., Zheng, Z.X., Zhao, G.S., 2022. Analytical models for heat transfer around a single ground heat exchanger in the presence of both horizontal and vertical groundwater flow considering a convective boundary condition. Energy 245, 123159.